Author/s:
Zhang, H;Liu, Y;Shahidan, MFS;Kinnear, C;Maasoumi, F;Cadusch, J;Akinoglu, EM;James, TD;Widmer-Cooper, A;Roberts, A;Mulvaney, P

Title:
Direct Assembly of Vertically Oriented, Gold Nanorod Arrays

Date:
2021-02-03

Citation:
Zhang, H., Liu, Y., Shahidan, M. F. S., Kinnear, C., Maasoumi, F., Cadusch, J., Akinoglu, E. M., James, T. D., Widmer-Cooper, A., Roberts, A. & Mulvaney, P. (2021). Direct Assembly of Vertically Oriented, Gold Nanorod Arrays. ADVANCED FUNCTIONAL MATERIALS, 31 (6), https://doi.org/10.1002/adfm.202006753.

Direct Assembly of Vertically Oriented, Gold Nanorod Arrays

Heyou Zhang[a], Yawei Liu[b], Muhammad Faris Shahin Shahidan[c], Calum Kinnear[d], Fatemeh Fatemeh Maasoumi[a], Eser Metin Akinoglu[a], Timothy James[e], Asaph Widmer-Cooper[b,f], Ann Roberts[c], and Paul Mulvaney[a*]

[a]ARC Centre of Excellence in Exciton Science, School of Chemistry, University of Melbourne, 3010, Victoria, Australia.

[b]ARC Centre of Excellence in Exciton Science, School of Chemistry, University of Sydney, NSW 2006, Australia.

[c]ARC Centre of Excellence for Transformative Meta-Optical Systems, School of Physics, University of Melbourne, 3010, Victoria, Australia.

[d]CSIRO Manufacturing, Ian Wark Laboratories, Clayton, 3169, Victoria, Australia.

[e]Reserve Bank of Australia, Craigieburn, Victoria.

[f]The University of Sydney Nano Institute, University of Sydney, Sydney, NSW 2006, Australia.

*e-mail: mulvaney@unimelb.edu.au

ABSTRACT:

Although many nanoscale materials such as quantum dots and metallic nanocrystals exhibit size dependent optical properties, it has been difficult to incorporate them into optical or electronic devices because there are currently no methods for precise, large-scale deposition of *single* nanocrystals. Of particular interest is the need to control the orientation of single nanocrystals since the optical properties are usually strongly anisotropic. Here we report a method based on electrophoretic deposition (EPD) to precisely assemble vertically oriented, *single* gold nanorods. We demonstrate that the orientation of gold nanorods during deposition is controlled by the electric dipole moment induced along the rod by the electric field. Dissipative particle dynamics simulations (DPD) indicate that the magnitude of this dipole moment is dominated by the polarizability of the solution phase electric double layer around the nanorod. The resulting vertical gold nanorod arrays exhibit reflected colours due to selective excitation of the transverse surface plasmon mode. The EPD method allows assembly of arrays with a density of over one million, visually resolvable, vertical nanorods per square millimetre.

This is the author manuscript accepted for publication and has undergone full peer review but has not been through the copyediting, typesetting, pagination and proofreading process, which may lead to differences between this version and the Version of Record. Please cite this article as doi: 10.1002/adfm.202006753.

KEYWORDS:

gold nanorods, arrays, electrophoretic deposition, plasmonic, vertical orientation, assembly, electric field induced dipole.

INTRODUCTION

Precision assembly of nanoscale materials is a crucial challenge limiting the advent of many potential nanotechnologies.[1]. Top-down fabrication is the most commonly used method to create nanostructures and allows direct integration into electronic devices.[2] However, in many cases, it is difficult to fabricate high quality nanostructures through top-down approaches. Consequently, bottom-up approaches, or hybrid approaches that combine top-down and bottom-up methods, are necessary.[3]

The easiest type of "bottom-up" assembly is the formation of nanocrystal superlattices, usually achieved by controlled solvent evaporation, and this has been used to generate superlattices with a moderate range of geometries, but it does not allow precise control over the relative arrangements of the particles.[4] DNA-mediation has also been used to expand the range of interparticle spacings. Only the application of external forces enables arbitrary assembly of nanomaterials and numerous methods have been investigated including: capillary force assembly (CFA),[5] chemically directed assembly (CDA),[6] dielectrophoresis,[7] optical tweezers,[8] magnetophoresis,[9] and electrophoretic deposition (EPD)[10].

Bottom-up assembly of *nanoscale* particles is substantially more difficult than is the case for larger particles, primarily because of Brownian motion. Most induced forces scale with particle volume so that larger particles are easier to manipulate. However, micron scale particles suffer faster rates of sedimentation, which can be a significant problem. Conversely, Brownian motion also helps the particles to sample many environments, which can help more stable assemblies to form and anneal defects. The key is obtaining the right balance between Brownian forces and the other forces driving the particles to assemble. Solomon and colleagues proposed that this is occurs for a Peclet number of Pe~1, i.e. assembly is most efficient when there is both advection or "particle forcing" and diffusion of nanoparticles.[11]

Here we use EPD because it can be applied to any charged colloid particle and in principle can be applied in both polar and non-polar solvents. EPD has commonly been used to deposit coatings

and dense, thin films of nanoparticles.[12] It has also been applied in microfluidic systems.[13] EPD of single particles has been demonstrated though it has been largely restricted to micron-scale particles. In our previous work,[14] we reported the direct assembly of large-area, single gold nanoparticle arrays via EPD, which pushed single-nanocrystal assembly to the nanoscale. It was demonstrated that EPD can be used to position *single* nanoparticles with nanometre resolution.

EPD requires well-defined surface charge densities for homogeneous deposition and works best for monodisperse particles. The DC field induces translational motion of a spherical particle at a speed that depends on particle size, shape, electrolyte concentration and surface charge.[15] For non-spherical particles, there is also a rotational force or torque generated due to the intrinsic polarizability of the material and also because of any permanent dipoles present within the material. The latter situation arises for CdS rods. Furthermore, a charged particle in solution is surrounded by a balancing diffuse layer of counterions. Polarization of this electrical double layer (EDL) also may be significant as we show. If the total rotational force can overcome Brownian forces, oriented deposition should be possible.[16]

In this article, we demonstrate the controlled deposition of single gold nanorods with a vertical orientation with respect to the substrate. We have investigated the influence of the electric field and gold nanorod size to generate high fidelity arrays. The optical properties of the vertical gold nanorods are characterized through dark field microscopy, and a millimetre scale array containing over 60 million vertical gold nanorods is assembled to demonstrate the scalability of the approach. Finally, COMSOL and dissipative particle dynamics (DPD) simulations are used to investigate the role of gold and electric double layer polarization on the nanorod orientation during EPD.

RESULTS

The fundamental question being addressed here is whether it is possible to control the orientation of a single nanocrystal during electrophoretic deposition (EPD). In a previous report, it was shown that individual gold rods could be deposited *horizontally* with nanoscale control over their positions and orientations.[14] However, horizontal orientation is expected for rods adsorbed at an interface. In this work, we investigate whether individual rods can instead be deposited *vertically* with a similar degree of control. In contrast to horizontal deposition, vertical deposition is unlikely to occur if the rods are randomly oriented as they approach the surface. The ideal outcome would be an array of rods deposited within a lithographically designed array, as shown in Figure 1(a).

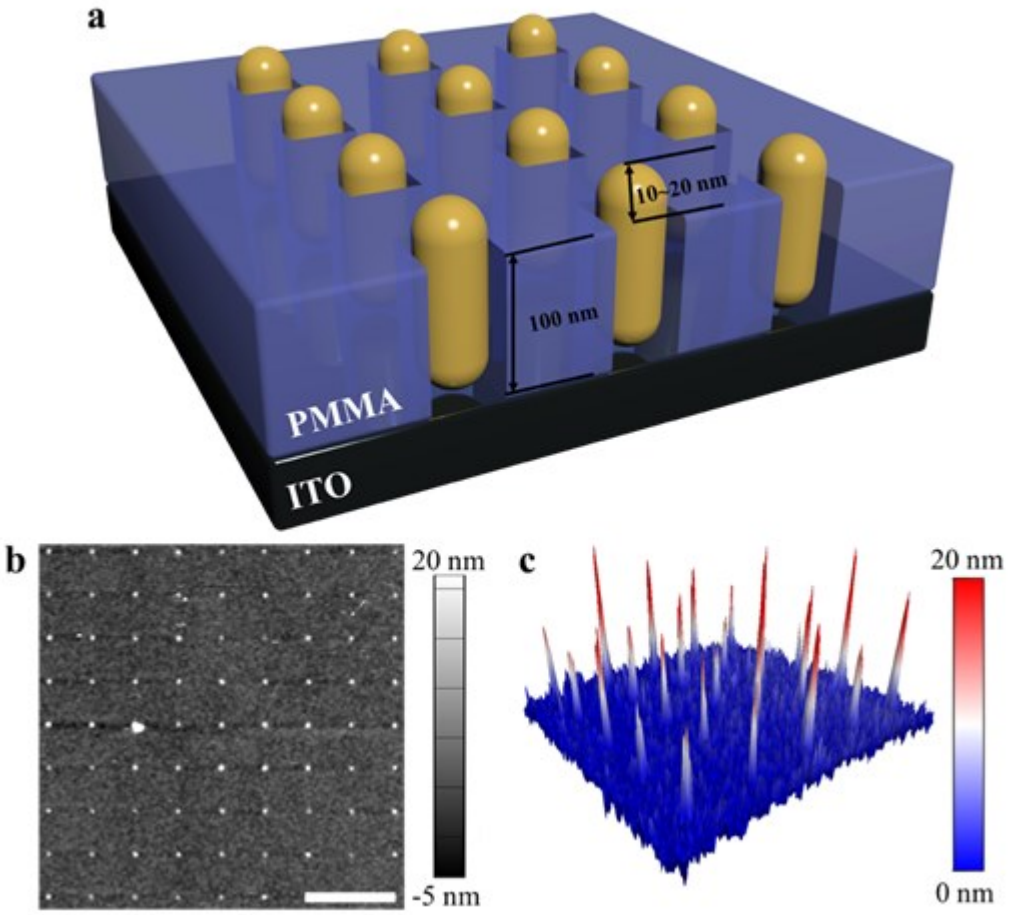

Figure 1. Vertical gold nanorod assembly *via* EPD (a) A schematic of the geometry of the vertically assembled gold nanorod array. The substrate is made from conducting transparent glass, and the PMMA layer is spin coated onto the substrate then etched via EBL. The cavity width should be 20-30% larger than the rod width. (b) Atomic force microscopy image of part of a gold nanorod array showing 9 · 9 vertically oriented gold nanorods (scale bar: 10 µm). (c) 3D coloured map of the height profile extracted from the atomic force microscopy image. The uniform spikes are around 15 nm high, showing that in each cavity the deposited rod protrudes from the cavity. The width of the spikes is consistent with single particle deposition (Colour bar: Height).

To investigate whether vertical assembly of individual rods is possible, EPD assembly was carried out using a template with square shaped cavities. The width of the square cavities was slightly larger than the width of a single gold nanorod but much smaller than its length. A 100 nm PMMA film was spin-coated onto pre-cleaned ITO glass. The cavities with size 50 × 50 nm were fabricated by electron beam lithography as described in the Experimental Section. Gold nanorods with a mean length of 113 nm and 42 nm width (NR113) were synthesised and assembled into the template via EPD. Because the length of the particles was longer than the depth of the cavities, after the assembly, the tips of the gold nanorods protruded from the surface and could be directly imaged by atomic force microscopy, as shown in Figure 1b. The interparticle spacing was 5 µm. Remarkably, nearly all the cavities were vertically filled with single gold nanorods. A 3D coloured height map was generated from the AFM image (Figure 1c). We observed that, on average, the gold nanorods protruded 14 nm above the surface with a minimum observed value of 10 nm and a maximum value

of 20 nm. The arrays were further characterized by scanning electron microscopy (SEM) as shown in Figure S2. There was a single gold nanorod particle in each cavity. From the normal view (Figure S2a and S2c), the circular shape of the rods was readily observed. When the viewing angle was reduced from perpendicular to 30° (Figure S2d) or 52° (Figure S2b), the "pillar" like particles standing inside the cavities and sticking out above the surface were more easily seen and clearly demonstrated that the arrays were constituted of single, vertically oriented, gold nanorods.

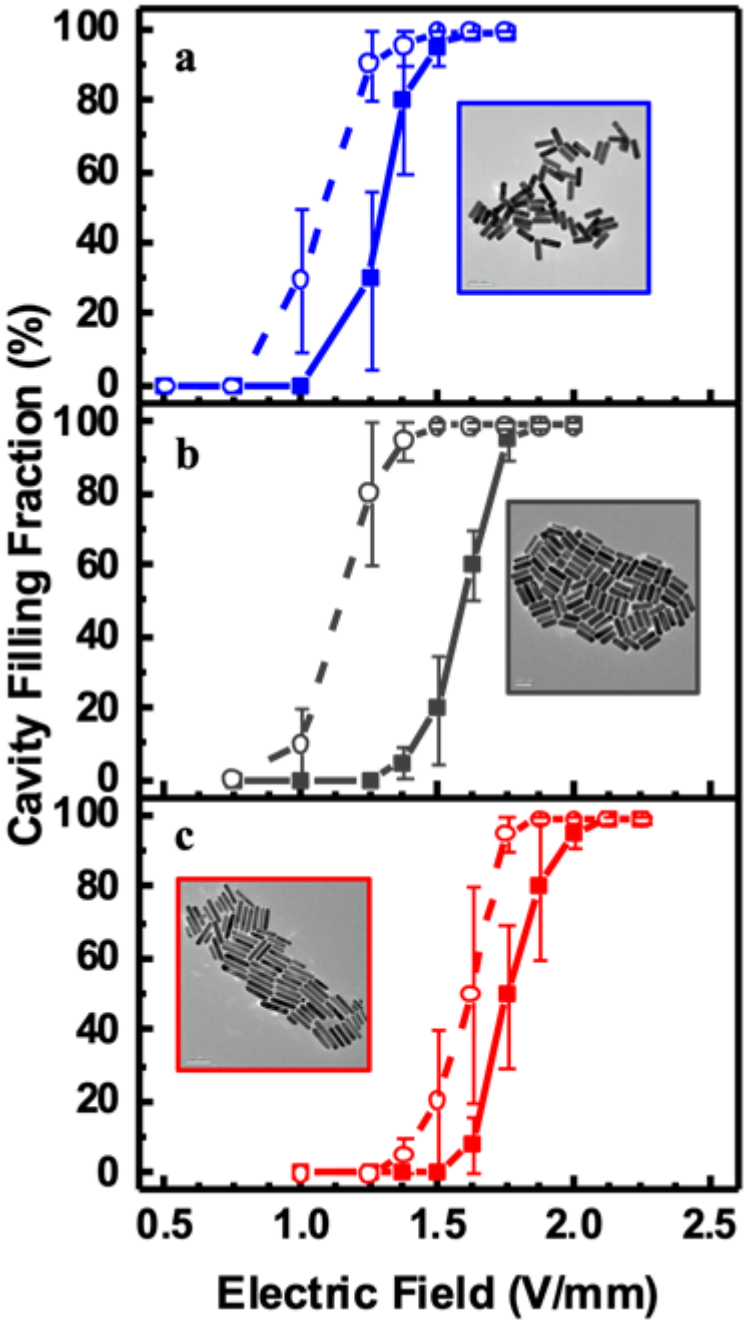

Figure 2. Filling Efficiencies during EPD. Plot of the cavity filling fraction in large (200 nm) cavities (hollow circles), and small (60 nm) cavities (solid squares) as a function of the electric field intensity (E) for three different sizes of gold nanorods. (a): NR160 with average length 160 nm and width 52 nm; (b) NR113 with average length 113 nm and width 42 nm and (c) NR95 with average length 95 nm and width 22 nm. (Gold nanorod concentration = 10 µg/mL,

salt concentration [NaCl] = 0.5 mM, temperature T = 293 K, pH = 7, aqueous phase). All error bars indicate the differences from the mean value from five assembly replicates for each data point.

The effects of rod aspect ratio and field strength were studied using templates with different sized cavities. Templates containing both large square cavities (200 × 200 nm) and small square cavities (60 × 60 nm) were used to assemble gold nanorods under a series of applied electric field strengths, and the filling fraction (defined as the ratio of filled cavities to the total number of cavities) was measured for both sizes of cavities, with the results shown in Figures 2a-2c. The time of each assembly attempt was fixed at 5s and the solution composition was fixed at 10 μg/mL for the gold nanorod concentration and 0.5mM for the NaCl concentration. The experimental filling fractions were determined by collecting dark field microscopy images after each experiment. Each of the data points is the result of 5 individual measurements across the substrate to minimise operator bias and errors associated with possible uneven electric field distribution across the template. The error bars show the difference in filling fractions across the five templates. Here, we focus on the influence of the applied electric field on the final orientation of the gold nanorods. Compared to the applied electric field, the electrolyte concentration has less effect on the orientation of gold nanorod but does significantly determine the magnitude of the local field.[14] Generally, a low electrolyte concentration leads to EPD and more non-specific adsorption (deposition on PMMA). High electrolyte concentrations lead to strong screening of both the template and particle surface charges, which may also result in low particle filling efficiencies as well as nanorod aggregation during EPD.

Figures 2a-2c show the influence of the electric field strength on the filling fraction for three different sized gold nanorods (Characterized in Figure S1) deposited into templates with either large (hollow circle) or small (solid square) cavities. For all three gold nanorod samples, the width of the large cavities was larger than the length of the gold nanorods. Hence, they could deposit with any orientation. As reported previously,[14] nanoparticles undergoing horizontal deposition require a minimum “turn on” electric field, to overcome the Brownian motion of the nanoparticle and other repulsive interactions related to the deposition. This was also observed here for vertical deposition. The rods exhibited an increasing “turn on” electric field of 0.75, 1, and 1.375 V/mm, for the rods of length 160 nm, 113 nm and 95 nm respectively. Deposition in this relatively low electric field regime resulted mostly in a random accumulation of gold nanorods and a significant number of empty cavities. Note that smaller rods required larger fields to initiate deposition. Because the rod widths were fairly similar, we attribute the effect to the differences in the rod length and, as will be shown later, it is the aspect ratio that is the important parameter. Furthermore, in all cases, the filling fraction approached 1 for large fields over a sharply defined range of field strengths. In the case of small cavities, the width was just large enough to accommodate the rods if they deposited vertically. We observed that the turn-on field strength shifted to higher values of 1, 1.375 and 1.75 V/mm in this case. The small cavities were found to contain individual, vertically oriented rods, while the larger cavities were found to contain multiple, vertically oriented rods.

Optical Properties of Vertical Gold Nanorod Arrays

The anisotropic optical properties of gold nanorods were also investigated for vertically assembled gold nanorod arrays. Due to the vertical geometry, we can directly observe the scattering signal of the plasma resonance of the short axis (transverse mode) for each vertical gold nanorod.

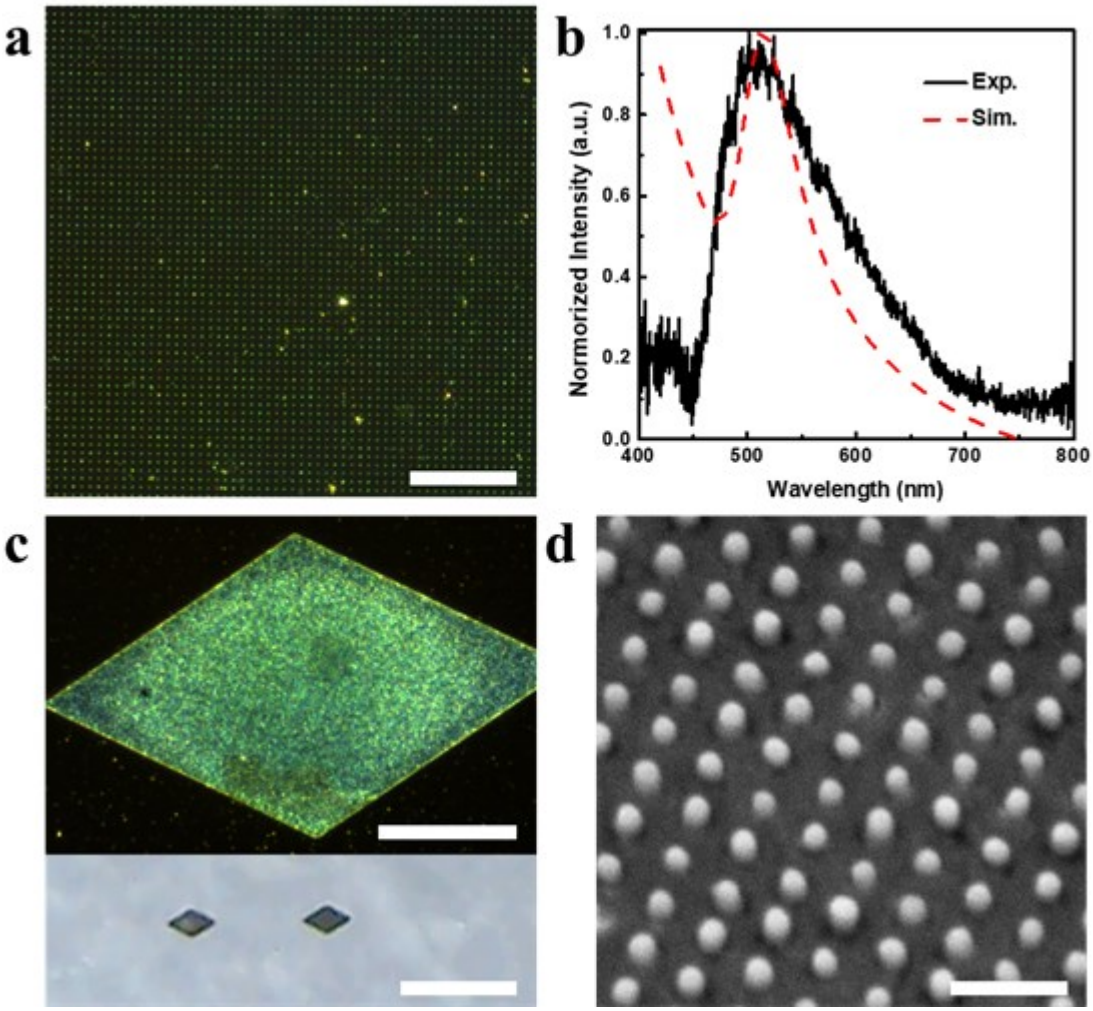

Figure 3. Optical properties of vertical gold nanorod arrays. (a) Dark-field microscopy image of an array with 50 nm square cavities filled with vertically oriented gold nanorods (Scale bar: 50 µm). (b) Corresponding single vertical gold nanorod scattering spectrum from the array in (a) (black line) and calculated single vertical gold nanorod scattering spectrum (Red dashed line). (c) Dark-field microscopy image (top, scale bar: 50 µm) and digital picture (bottom, scale bar: 500 µm) of a hexagonal array consisting of vertically assembled gold nanorods with 200 nm spacing. (d) corresponding SEM image of the hexagonal array with 52° tilted viewing angle (scale bar: 500 nm).

Dark field microscopy was used to characterize the light scattering from the vertical gold nanorod arrays. Figure 3a shows a dark field microscopy image of an array filled with vertically oriented gold nanorods (NR113). The template was comprised of 50 × 50 nm cavities with 100 nm PMMA thickness. The centre-to-centre distance between each row and column was 5 µm. This spacing allowed us to observe the optical response of each individual particle assembled, since near-field optical coupling of nanoparticles is dependent on the distance between the particles. As shown in Figure 3a, a uniform film was created which exhibited greenish light scattering. The green colour is due to the scattering of light from the transverse surface plasmon mode of the gold nanorods and indicates that the array was filled exclusively with vertically oriented rods. Some yellow and red scatter spots were also observed which are caused by the aggregation and misalignment of rods on the PMMA background respectively. As we reported previously,[14] this mis-assembly was due to the high potential applied during the EPD process for vertical orientation, which increased the chance of particle mis-deposition and aggregation on the surface of PMMA. Figure 3b shows the normalized scattering spectrum from a single vertical gold nanorod measured with dark field microscopy (black line) and also the spectrum simulated using the Finite Element Method as implemented in COMSOL Multiphysics (red dashed line). Due to limitations in the detector response and the relatively low scattering intensity of the transverse mode, the spectrum we measured using dark field microscopy was relatively noisy and the signal cut off at 450 nm. The spectrum, however, still evinced a clear scattering peak at 530 nm, which is close to the transverse mode peak measured for the ensemble using UV-Vis spectrophotometry (Figure S1 NR113) and to the peak in the simulated scattering spectrum.

In order to create stronger optical contrast, a separate template was constructed with cavities arranged in a denser, hexagonal array with 200 nm edge-to-edge distance. Figure 3c shows the dark-field microscopy image (top) and digital picture (bottom) of this “diamond”-shaped array filled with vertically oriented gold nanorods. Due to the higher packing density, the dark-field microscope image exhibited a stronger green colour scattered from the “diamond” array compared to the lower density array shown in Figure 3a (for the scattering spectrum, see Figure S3a). The green colour could even be directly observed under natural daylight, with the help of a 200× magnification digital microscope camera, as shown in Figure 3c (bottom). The length and width of the “diamond” array were approximately 0.2 mm and 0.1 mm respectively. Figure 3d and Figure S3b-S3e show scanning electron microscope images of the “diamond” arrays. From the normal viewing angle (Figure S3b, S3c), each particle looked “round” since the short axis of the nanorods was observed. Nearly 99% of cavities were filled with particles. When the viewing angle was changed to 52°, the vertically oriented nanorods were clearly visible, as shown in Figure 3d and Figure S3d-S3e. Because the average length of the gold nanorods was generally 10~20 nm longer than the thickness of the PMMA, part of the gold nanorods protruded from the PMMA surface. Note that, due to the inhomogeneous distribution of lengths and widths of the gold nanorods in Figure 3d and Figure S3, “tall” and “short” gold nanorods are observed.

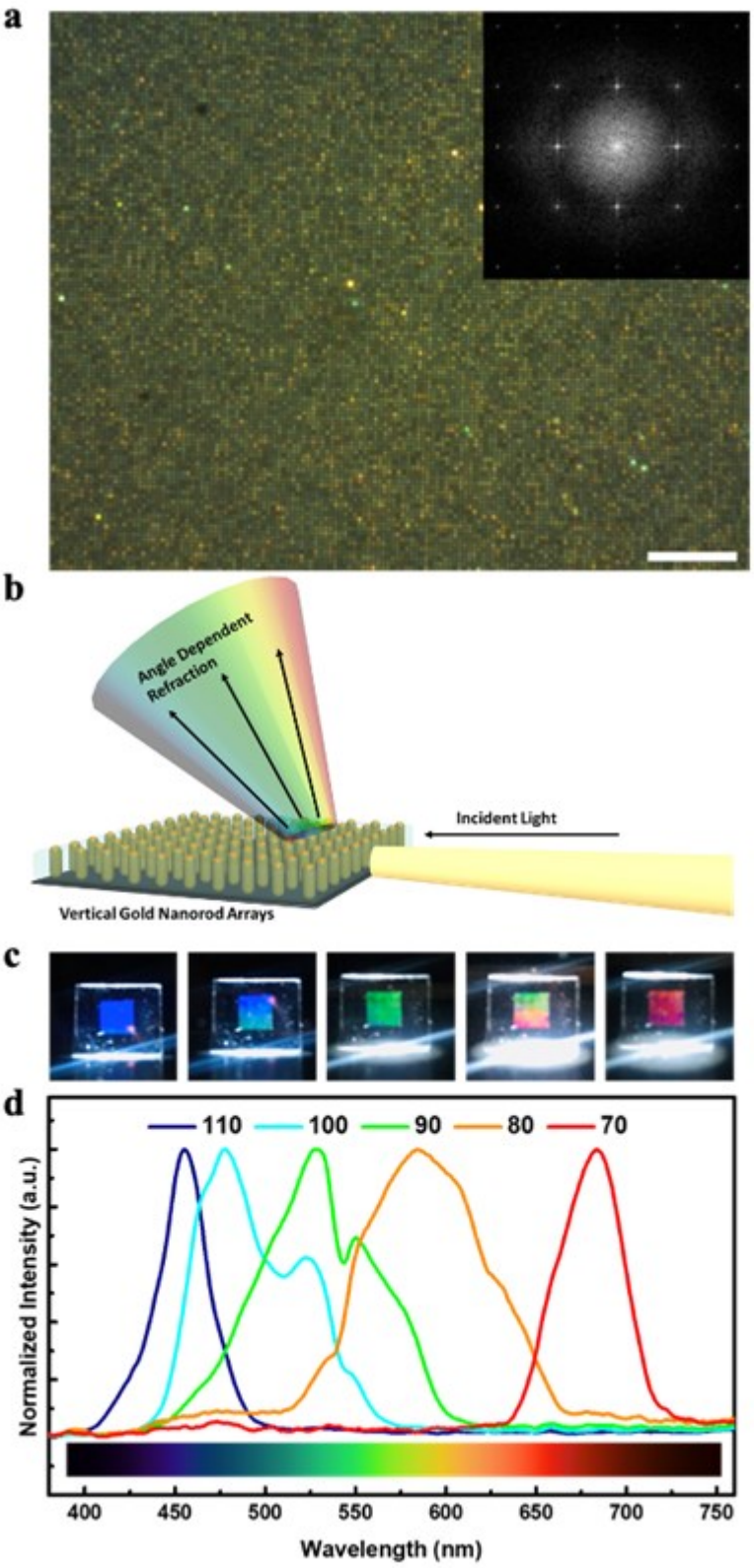

Figure 4: Large area vertical gold nanorod arrays. (a) Dark-field microscopy image of an array of vertically assembled gold nanorods with 500 nm spacing (Scale bar: 10 μm) and Fast Fourier Transform (FFT) of the dark-field microscopy image (insert). (b) A schematic of the measurement setup used to collect the scattered light spectrum from the vertical gold nanorod array. (c) Digital pictures of the 4 mm × 4 mm vertical gold nanorod array at different viewing angles from 110° (left) to 70° (right). (d) Normalized refracted light spectra of a vertical gold nanorod array for different collection angles.

EPD enables the assembly of nanoparticles on even larger scales. A 4 mm by 4 mm template was constructed on a 1 cm by 1cm ITO-PMMA slide, consisting of 8000 × 8000 cavities of size 60 × 60 nm with 500 nm spacing. Under a dark field microscope equipped with a LU Plan Fluor 100×A/0.90 Nikon lens, it was possible to resolve individual particles in the assembled nanorod array, as shown in Figure 4a. Each of the individual yellowish green dots represents a single, vertical, gold nanorod. Uniform green scattering over the array indicates large-scale control of the orientational order. More than 99% of the cavities were filled with a single vertical gold nanorod, with a small number of aggregates evident as bright, yellow dots, and a few empty cavities visible as dark voids. The inset in Figure 4a is a Fast Fourier Transfer (FFT) of the dark field image. The clear, isolated spots provide evidence for the large scale square ordering of the particles.

To further characterize the optical properties of such large-area, vertical gold nanorod arrays, an experiment was designed to measure the scattering of light through the array. A photo of the experimental setup is shown in Figure S5, with a schematic shown in Figure 4b to illustrate the measurement. A deuterium-halogen light source was used as a white incident light to illuminate the vertical arrays. The light source was channelled by an optical fibre and was incident from the side of the template slide. As the white light propagated through the square array from one edge to the other, the incident light refracted above the array was detected by another optical fibre connected to a spectrometer. The spectrum was measured at a set of fixed angles between the detector fibre and the incident light. The angle dependent spectra are shown in Figure 4d along with pictures (Figure 4c) taken at the corresponding angles. The spectrum of colours from red to green and blue were observed across the entire arrays as the viewing angle was altered from 70° to 110°. The collected spectra of the scattered light are consistent with the colour we observed by eye, with the peak shifting from approximately 680 nm (red) to 530 nm (green) to 450 nm (blue) as the angle was changed from 70° to 90° to 110°. At 80° and 100°, in Figure 4c, we observed a mixture of colours across the array. At 80°, the array exhibited green-yellow-red colours from the top of the array (the side of the light incident) to the bottom. Similarly, at 100° the array exhibited blue-cyan-green colours in the same order. This phenomenon is caused by a difference in the viewing angle across the array. The angle was larger at the edge of the array where the light was incident and smaller at the opposite edge of the array. Those mixtures of colours are also reflected in the spectra we measured at those two angles, shown in Figure 4d. At 80°, a broad peak was observed from 520 nm to 660 nm, which corresponds to colours ranging from green to red; and at 100°, a broad peak was observed from 440 nm to 550 nm, which covers the colours from blue to green. In addition, in the spectra measured at 80°, 90°, and 100°, there is a side peak at approximately 530 nm that is angle independent. This peak is attributed to scattering from the transverse plasmonic resonance of the

gold nanorods[17]. In the absence of the gold rods, only a very weak scattered beam was observed due to the diffraction of light from the empty cavities.

DISCUSSION:

The results presented here demonstrate unambiguously that during electrophoresis, it is possible to control the orientation of the rod during migration in the electric field. This makes it possible to precisely position single gold rods in suitable cavities with controlled orientation. In order to generalise our results, it is useful to consider what parameters affect the orientation of the particles and the filling fraction since these are the most important practical properties of interest.

In solution, charged colloidal particles are surrounded by a diffuse cloud of counterions in which the charge density decays exponentially with distance from the surface. Taken together, the surface charge and the diffuse cloud, called the electric double layer (EDL), are a neutral body. Whenever an electric field is applied, the charged particle experiences a force in one direction while the diffuse cloud of counterions experiences a force in the opposite direction. This changes the distribution of ions around the particle and results in polarization of the EDL. At the continuum level, the electrophoretic velocity is determined by the balance of the electric force and the hydrodynamic friction on the particle and is usually proportional to the strength of the external electric field.[15a, 18] At the microscopic level, Brownian dynamics and diffusion are also important, which explains why a minimum electric field strength (E_{min}) needs to be applied before the cavities start to fill, as shown in Figures 2a-2c. The observation that E_{min} increases as the rods become smaller can similarly be rationalized by their smaller total surface charge.

To understand how the rods are able to enter the smaller cavities to form vertical assemblies, however, we need to consider the torque that the external electric field exerts by acting on the charge distributions present both within the rods and near their surface. In the rest of this section, we therefore characterize the dipoles induced inside the gold nanorods and within the EDL and discuss their relative magnitudes and effect on the rod orientation.

According to previous reports,[19] under an external electric field $\vec{E}$, gold nanorods exhibit an induced dipole moment $\vec{p}_{Au}$

$$\vec{p}_{Au} = \alpha\vec{E} \quad \text{eq.1}$$

where α is the polarizability tensor of the particle, which is dependent on the volume of the particle, aspect ratio and dielectric permittivity (see Supporting Information). To simplify the expression, we treat the gold nanorod as a spheroid which has the longitudinal polarizability $\alpha_{\parallel}$ along the long axis and the transverse polarizability $\alpha_{\perp}$ along the short axes. Then the torque $\vec{\tau}$ applied on a nanorod under the external electric field is given by:

$$\vec{\tau} = \vec{p}_{Au} \times \vec{E} = -\Delta\alpha_{Au} \times cos\ cos\ \theta\ \times sin\ sin\ \theta\ \times E^2 \qquad \text{eq.2}$$

where $\Delta\alpha_{Au} = \alpha_{\parallel} - \alpha_{\perp}$ and θ is the angle between the electric field vector and the long axis of the nanorod. This torque will drive the gold nanorods to align with the electric field, i.e. it will rotate them towards θ = 0, with a force proportional to the square of the applied field strength. In competition with this, Brownian motion will act to randomize the orientation of the nanorods. For a fixed rod size ($\Delta\alpha_{Au}$ constant), a stronger electric field will therefore produce a stronger torque and thus a higher probability of nanorods aligning with the local electric field during the EPD process, which is essential during the final stages in order for the rods to fill the narrow cavities and achieve a 100% vertical filling fraction. Consistent with this, we find that a higher electric field is needed to fill the small cavities than the large ones (compare the closed and open symbols in Figures 2a-2c).

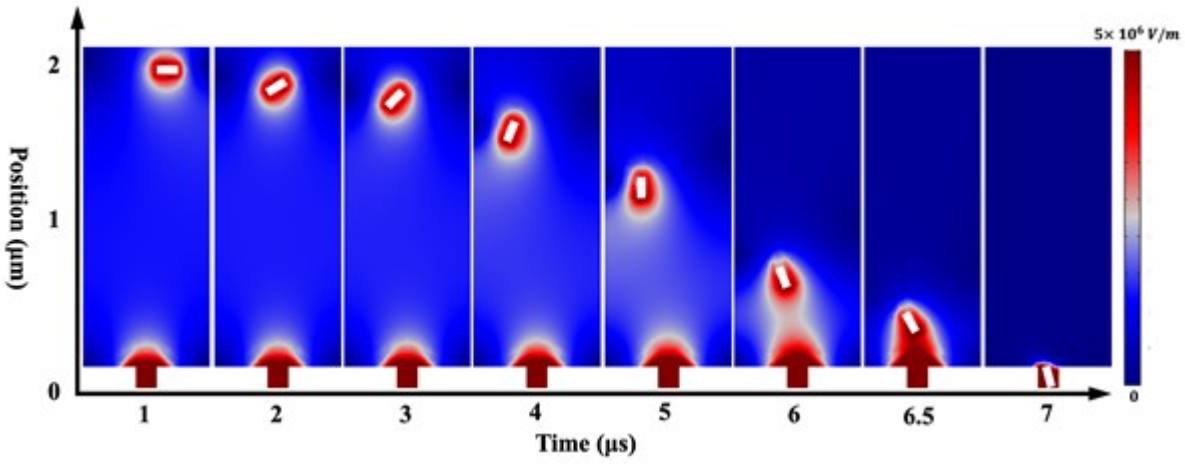

Figure 5. COMSOL Multiphysic simulation results. Time-dependent simulation of a single rectangular gold particle moving in water under the influence of an electric field. A potential of −1.5 V was applied at the bottom of the cavity, and the zeta potential of the particle was set to + 50 mV. No electrolyte is applied in the aqueous solution. (Colour bar: Electric field strength V/m).

To demonstrate that this can guide particles into the cavities, a simplified model was built in 2D with COMSOL Multiphysics to explain vertical deposition of nanorods during EPD (Figure 5). This model incorporates both the electric fields and also the solution phase dynamics of the problem and is a time-dependent simulation of a charged gold rod moving in water under the influence of an electric field. The model was built with a single cavity (100 nm in width and 100 nm in depth). A -1.5 V potential was applied at the bottom of the cavity, the top and sides of the cell were grounded, and a rectangular gold particle (100 nm in length and 40 nm in width) was placed 2 µm above the cavity. The zeta potential of the particle was set to + 50 mV, similar to the values we obtained experimentally. The results show that under the influence of the external field, the particle moves towards the cavity while rotating to align with the local electric field. This allows the rod to be guided into the cavity and ultimately deposit with a nearly vertical orientation, consistent with what we observed experimentally. During this process, the electric field around the particle is gradually

distorted, becoming higher at the end closest to the cavity and lower at the other end due to the electric dipole induced within the particle (e.g. see t = 5μs). The presence of electrolyte would reduce the field experienced by the rod, but the overall process should remain qualitatively the same.

According to eq.2, the torque is proportional to the difference in the polarizabilities along the long and short axes ($\Delta\alpha_{Au}$), which suggests that higher aspect ratio rods will be easier to align. This may explain why the difference in the field strengths needed to fill the small and large cavities (see Figures 2a-c) is largest for the rods with the smallest aspect ratio (NR113) and smallest for the rods with the largest aspect ratio (NR95). The polarizabilities calculated for our gold cores are summarized in Table 1 and were obtained as described in the Supporting Information.

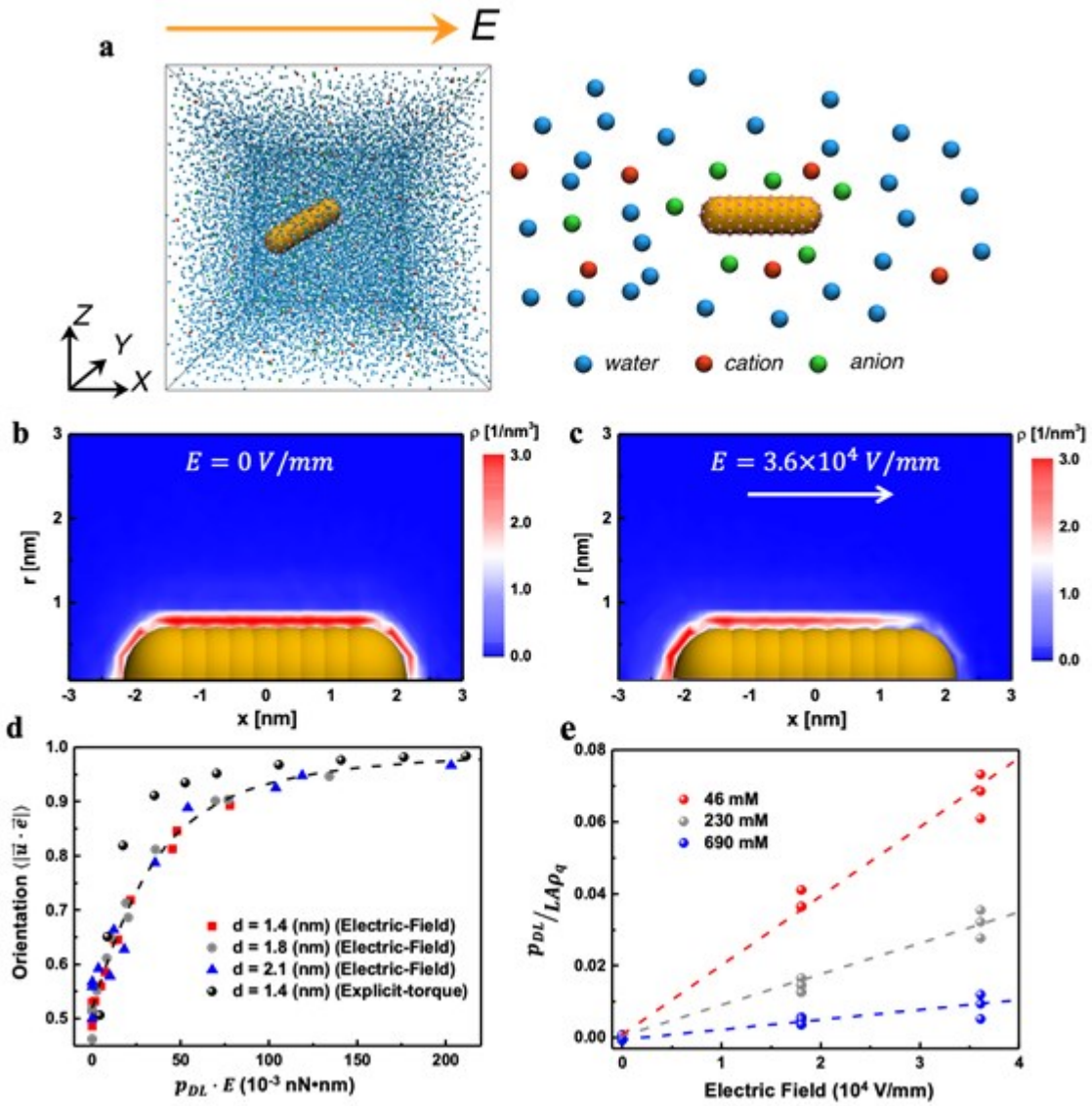

Figure 6. Dissipative particle dynamics simulations of a charged nanorod in an electrolyte solution under the influence of a DC electric field. (a) Illustration of the model used in the simulations. The periodic simulation cell was filled with coarse grained water molecules (blue spheres), cations (red spheres), anions (green spheres) and one rigid nanorod with positive surface charges (1.2 e/nm^2). The nanorod was constructed from overlapping spheres with diameter d and had a fixed aspect ratio of 3. An electric field E was applied across the box along the +x direction. (b,c) Density profile of anions around the nanorod for E = 0 and $3.6 \cdot 10^4$ V/mm, respectively. The concentration of 1:1 electrolyte was 46 mM. (d) The time-averaged nanorod orientation (parallel to the field = 1) as a function of the torque applied to the nanorod. Three different sizes of nanorod were simulated, with 1.4 nm (red squares), 1.8 (grey spheres), and 2.1 nm (blue triangles). The applied electric field varies from 0 to $5.4\ 10^2$ V/mm for each nanorod. An explicit torque was also applied to a d = 1.4 nm nanorod (black spheres) and plotted for comparison to the other, electric-field induced, torques. (e) Plot of the normalized dipole moment of the electric double layer as a function of the external electric field for three different electrolyte concentrations.

There are two sources of electrical polarization. The first is from the particle itself and arises largely from the polarization of the free conduction electrons in the gold metal. The second is from the relative motion of the ions forming the diffuse double layer around the particle. While the electron density of the metal is higher, the potential displacement of double layer ions is larger. To compare the polarization of the electric double layer with the polarization of the metallic gold core, and to characterize its role in orienting the rods during EPD, we used dissipative particle dynamics (DPD) simulations. The basic model used in our DPD simulations is shown in Figure 6a. The system consists of one positively charged rigid nanorod placed inside a box with periodic boundary conditions in all three directions. This rod was constructed from overlapping spheres with a fixed aspect ratio of 3 (total length/sphere diameter).[20] The surface charge density of the rod was set to $1.2\ e/nm^2$ (i.e. $\sim 0.19\ C/m^2$), which is close to the reported packing density of CTA^+ on gold surfaces.[21] (For a discussion of the appropriate surface charge density to compare with the experimental results, see the DPD section of the SI.) The water and ions in the system were modelled as DPD beads with one water bead representing 4 water molecules and one ion bead representing 3 water molecules plus 1 cation or anion (see Figure S7). The concentration of electrolyte was controlled by the ratio of water to ion beads inside the box, and an external electric field was applied in the +x direction. More details about the model, including how the parameters used were converted to real units, are provided in the Supporting Information.

As shown in Video 1, when a suitably large electric field is applied, the rod spontaneously aligns with the field direction and undergoes electrophoretic motion along it. We have characterized, as a function of field strength, the orientation of the rod along with the orientation and magnitude of the dipole formed by distorting the counterion cloud (see Figure S9 in the Supporting Information). For the nanorod with a diameter of $1.4\ nm$ at a salt concentration of 46 mM, only random Brownian

motion is observed at E = 0. At E = 0.9 × 10^4V/mm, the nanorod starts to move along the direction of the electric field (+x direction), and at E = 1.8 × 10^4 V/mm the rod starts to show a preference for orienting parallel to it ($\langle|\vec{u}\cdot\vec{e}|\rangle > 0.6$), while at E ≥ 3.6 × 10^4 V/mm the rod remains strongly oriented as it moves parallel to the electric field ($\langle|\vec{u}\cdot\vec{e}|\rangle > 0.8$). While this field strength is 4 orders of magnitude larger than the average field in the experiments (see Figure 2), it is only 1-2 orders of magnitude larger than the field near the cavity in the COMSOL simulation shown in Figure 5. In addition, the rods in our DPD simulations are much smaller than the experimental ones due to size limitations (about 3 orders of magnitude by volume). This means that a proportionally larger electric field is needed to orient them, which explains the apparent difference in field strengths, as we shall discuss in detail below.

The density profile of anions around the nanorod at E = 0 and E = 3.6 × 10^4 V/mm are shown in Figures 6b and 6c, respectively. When there is no external field, the anion counterions are evenly distributed around the surface of the nanorod. However, at E = 3.6 × 10^4 V/mm, the counterions have redistributed themselves to form a strong density gradient along the length of the rod which, together with the charges on the rod surface, form an electric dipole that points in the opposite direction to the applied field. Similar to the dipole induced in the gold core, this dipole induced in the EDL can apply a torque on the nanorod and contribute to orienting it during EPD. We will refer to the electronic dipole moment associated with the distribution of charges in the EDL as $\overrightarrow{p_{DL}}$. Figure 6d shows the relationship between the nanorod orientation and the torque applied on the nanorod due to $\overrightarrow{p_{DL}}$. The orientation here is calculated as $\langle|\vec{u}\cdot\vec{e}|\rangle$, where $\vec{u}$ is a normalized vector pointing along the long axis of the nanorod, $\vec{e}$ is a normalized vector pointing in the direction of the electric field, and $\langle\rangle$ indicates a time average. The torque is calculated as $\overrightarrow{p_{DL}}\times\vec{E}$,where $\vec{E}$ is the electric field vector and $\overrightarrow{p_{DL}}$ is the dipole moment formed in our simulations under the influence of the electric field. Three different sizes of nanorods were simulated (by changing the diameter), with all three exhibiting the same nonlinear relationship between orientation and electric field induced torque. As the torque is increased, the average orientation of the nanorod first changes rapidly and then asymptotes towards a configuration with the long axis parallel to the electric field. Similar behaviour was obtained by directly applying an explicit torque to one of the nanorods without the electric field.

In order to compare the polarizabilities of the gold core and the EDL, and thus their relative importance for achieving vertically oriented EPD, we investigated the relationship between E and p_{DL} (the magnitude of the dipole induced in the EDL). Figure 6e shows $p_{DL}/(LA\rho_q)$ as a function of the applied field strength for three different rod sizes and ionic strengths, where L and A are the rod length and surface area, respectively, and ρ_q is the surface charge density obtained from the simulations. As can be seen, the normalized EDL dipole moment is proportional to the applied electric field for all three concentrations, independent of rod size. Hence, we propose the relationship:

$$p_{DL} = \alpha_0 \cdot LA\rho_q \cdot E \qquad \text{eq.3}$$

where α_0 is the slope of the linear fitting in Figure 6e for a given electrolyte concentration. For the three concentrations simulated, we obtained $\alpha_0(46\ mM) = (1.92\ \pm 0.06)\ \times\ 10^{-9}\ m/V$, $\alpha_0(230\ mM) = (0.86\ \pm 0.03)\ \times\ 10^{-9}\ m/V$, and $\alpha_0(690\ mM) = (\ 0.25 \pm 0.03)\ \times\ 10^{-9}\ m/V$. Fitting this with an exponential function provides a rough lower bound for α_0 at the experimental electrolyte concentration of $\alpha_0(0.5\ mM) \approx\ 2.1\ \times\ 10^{-9}\ m/V$.

We can now estimate the polarizability of the EDL in the experimental parameter regime by using $\alpha_{DL} =\ \alpha_0 \cdot LA\rho_q$. Scaling up the size is straightforward, but there is considerable uncertainty about the appropriate surface charge density to use, given that this cannot be directly measured experimentally (see the DPD section of the SI for an in-depth discussion). We have therefore calculated a range of possible values, with the most likely result falling somewhere in the middle. The results using the dimensions of our three gold nanorod samples are listed in Table 1 together with the polarizabilities of the gold cores $\Delta\alpha_{Au}$. This means that all three α_{DL} values are at least comparable to, and possibly two orders of magnitude higher than, $\Delta\alpha_{Au}$ and $\alpha_{||}$, the component of $\Delta\alpha_{Au}$ directed along the length of the rod. This range is consistent with previous research, in which the experimental estimate for the polarizability of gold nanorods stabilized by CTAB was ~30 times higher than that expected for the gold cores.[19b] This indicates that the dipole induced in the EDL is more important than the one induced in the gold core for orienting the nanorods parallel to the electric field during EPD. It also suggests that with proper electrolyte concentration and surface charge density it may be possible to use EPD to assemble vertical arrays of nanorods with no intrinsic dipole and low intrinsic polarizability, such as PbS nanorods,[22] polystyrene ellipsoids[11a] and nanofibrillated cellulose.[23]

Note that our simulations (COMSOL and DPD) are only a preliminary prediction of the movement of charged anisotropic particles under the influence of an electric field. For a more accurate prediction, more effects will need to be considered including the ligand/polymer shell structure, electroosmosis, and the electric field distribution within the experimental setup.

Table 1: Polarizabilities calculated for the three nanorods used in the experiments: values obtained for the gold core ($\Delta\alpha_{Au}$ and $\alpha_{\|}$) and the electric double layer (α_{DL}) are reported separately to allow for comparison. In the calculation of α_{DL}, a CTAB double layer with thickness of 4 nm was taken into account when scaling up the simulation results, as a lower limit on the thickness of the ligand/polymer shell. The lower and upper limits for α_{DL} were obtained at surface charge densities of $0.02\ e/nm^2$ (i.e. $\sim 0.003\ C/m^2$) and $1.2\ e/nm^2$ (i.e. $\sim 0.19\ C/m^2$), respectively (with a detailed discussion for this range provided in the SI).

	Mean Length (nm)	Mean Width (nm)	$\Delta\alpha_{Au}$ (F•m^2)	$\alpha_{\|}$ (F•m^2)	α_{DL} (F•m^2)
NR160	160	52	1.94×10^{-32}	2.54×10^{-32}	$(3.6 - 215) \times 10^{-32}$
NR113	113	42	6.99×10^{-33}	9.73×10^{-33}	$(15.4 - 922) \times 10^{-33}$
NR95	95	22	3.66×10^{-33}	4.29×10^{-33}	$(6.7 - 400) \times 10^{-33}$

CONCLUSIONS

In this work, we have explored and demonstrated that electrophoretic deposition can be used to assemble large arrays of vertically oriented nanorods with precise control of position at the single particle level. By using box cavities with the appropriate size, gold nanorods can be oriented and deposited vertically on the patterned PMMA-ITO substrate. The resulting vertical array allows us to explore the plasmonic and optical properties of such unique structures from the nanoscale right up to millimetre length scales. The key factor that controls the orientation of the nanorods (which have no permanent dipole) is the magnitude of the dipole induced along the rod axis by the external electric field. Both the polarizability of the gold core and the polarizability of the electric double layer can contribute to the induced dipole. While both of these contributions exhibit trends that correlate with the experimental results, our analysis suggests that polarizability of the electrical double layer (EDL) is the dominant effect in our case. This implies that it should be possible to use EPD to assemble vertical nanorod arrays using a wide range of materials (including ones that do not have strong intrinsic dipoles or polarizability), as long as the surface charge of the nanorods and the polarizability of the EDL can be sufficiently enhanced. This would greatly extend the practical value of EPD assembly in nanomaterials fabrication and associated technologies.

METHODS

Synthesis of gold nanorods with three different sizes

Three types of gold nanorods were synthesized using the binary surfactant method whereby different reagent ratios are used to control the size[24]. To create gold seeds, 5 mL of 0.5 mM $HAuCl_4$ aqueous solution (prepared from $HAuCl_4 \bullet 3H_2O$ (Sigma-Aldrich 99.9%)) was added into a vial, followed by 5 mL of 0.2 M CTAB aqueous solution (Sigma-Aldrich, ≥98%). After 2 mins of slow stirring (400 rpm), 0.3 mL of 20 mM freshly prepared $NaBH_4$ (Sigma-Aldrich, ≥98%) was added under vigorous stirring (1,200 rpm). The solution turned brown instantly which indicated the formation of gold seeds. After 5 min stirring, the resultant seed solution was aged at room temperature for at least 30 mins before use. Three different sizes of gold nanorods were prepared using the reagent ratios shown in Table 2. In general, CTAB and NaOL (sodium oleate, Sigma-Aldrich, ≥99%) were added into a 1 L round flask. 250 mL water was then added into the flask and heated at 50 °C under stirring (500 rpm) to dissolve the CTAB and NaOL. Then, the flask was cooled down and maintained at 30 °C during the rest of the procedure. After the temperature had stabilised, the required volume of 4 mM $AgNO_3$ (prepared from $AgNO_3$ powder, Sigma-Aldrich, ≥99%) was added into the flask and mixed by stirring. 250 mL of 1 mM $HAuCl_4$ solution was then added into the flask. The solution was left undisturbed for 15 min at 30 °C. After that, the solution was kept stirring at 700 rpm for 90 mins until colourless. Concentrated HCl was added to adjust the pH. Then 1.25 mL of freshly prepared 0.1 M L-ascorbic acid (Sigma-Aldrich, reagent grade) were added to the solution, under vigorous stirring (1200 rpm) for 30 s. Finally, the appropriate volume of gold seed solution (see Table 2) prepared previously was added while stirring. The solution was then left undisturbed overnight at 30 °C. The final product was centrifuged for 20 min and redispersed in 5 mM CTAB solution. To overcoat the gold nanorods with p-DADMAC, 2mL of the gold nanorod solution with an approximate concentration of 50 μg/mL was centrifuged at 2000 rcf and redispersed in 2 mL of Milli-Q water.

Then 1 mL of 10 mM NaCl solution was added into the solution with stirring (500 rpm). A mixture of 2 mL 1% polystyrene sulfonate (PSS) solution and 1 mL 10 mM NaCl solution was then added to the particle solution while stirring. After 5 min, the solution was left undisturbed for 30 min followed by centrifugation at 1500 rcf. The precipitate was then redispersed in 2 mL of Milli-Q water and the same steps were repeated but using 1 % p-DADMAC solution instead of PSS solution. The structural characterization of the gold nanorods is summarized in Figure S1. Zeta potentials were determined using a Brookhaven Zeta PALS instrument and were found to be + 50 mV ± 3 mV. We choose p-DADMAC to coat the gold nanorods for the following reasons. (1) A polymer coating on gold nanorods can increase the colloid stability and eliminates the need for free ligands, For example surfactants also alter the electrolyte concentration. (2) p-DADMAC provide a relatively high surface charge. (3) p-DADMAC renders the gold nanorod positively charged. We deposit positively charged gold nanorods onto negatively charge electrodes to eliminate the possibility of electrochemical oxidation of the gold rods.

Table 2: Volumes of reagents used to synthesize gold rods of different aspect ratio. Histograms are shown in Figure S1.

	CTAB Mass	NaOL Mass	$AgNO_3$ Volume	HCl Volume	Gold Seed Volume	Mean Length (nm)	Mean Width (nm)	Aspect Ratio
NR160	9 g	1.23 g	24 mL	3.6 mL	0.01 mL	160	53	3.05
NR113	9 g	1.24 g	24 mL	1.5 mL	0.1 mL	113	42	2.70
NR95	9 g	1.23 g	36 mL	3 mL	0.2 mL	95	22	4.31

Template Patterning

The templates were patterned with electron-beam lithography (EBL). ITO-glass slides (Lumtec Technologies Corp LT-G001ITO Glass 15Ω) were cleaned by rinsing them with 2-propanol (IPA) and water. Then a 100 nm PMMA resist layer was deposited by spin coating PMMA (A2) at 1000 rpm onto the ITO and baked at 180 °C for 5 mins. A 30 nm thick chromium layer was then sputtered onto the PMMA-ITO slide using a Sputter Coater (Cr Quorumand) To pattern the ITO-PMMA template, the slides were exposed to an electron-beam (Vistec EBPG 5000plus ES) using 1nA current, 300 µm aperture, and a 100 kV accelerating voltage. A custom pattern was created using modelling software (Klayout). After exposure, the chromium layer was removed by immersion for 1 min in a Cr etching solution, followed by 5 sec in 5% H_2SO_4 and then applying a water rinse. The pattern was then developed with 3:1 methyl isobutyl ketone (MIBK) and IPA for 1min and then the slide was finally rinsed with IPA three more times, followed by a further water rinse and blown dry with nitrogen gas.

EPD Cell assembly

The EPD assembly cell was similar to the one previously used.[14] In brief, the three components (Top cover, bottom cover and middle chamber) of the EPD cell were fabricated by 3D printing (TEVO Black widow) using polylactic acid (PLA), at a printing temperature of 220^{o}C. The printing layer thickness was 0.2 mm. The top and bottom pieces of the cell were printed as full solids with 1 mm thickness for better fluid sealing. The rest of the cell was printed using a zigzag structure with a 30 % filling rate to construct the body. The EPD chamber comprised a region 5 mm (L) × 5 mm (W) × 2 mm (H) in the middle section of the cell. The cell was sealed by placing Teflon tape between the cell and ITO slides and tightened with four screws at the respective corners. The gold nanorod solution (10 µg/mL) containing 0.5 mM NaCl was injected into the cell from the side channel through an injection port. The injecting process needed to be slow and gentle to prevent air bubbles forming and to avoid leaking of the colloid. For the EPD process, the template and counter electrodes were both connected to a potentiostat (Metrohm AutoLab). A constant DC potential was applied for a fixed time period. After deposition, the template was washed by gently flushing water over the surface and then blow drying with nitrogen.

Spectroscopy

Dark field scattering spectra and images of the vertical gold nanorod arrays were collected with a Nikon Lv100 Eclipse inverted microscope, equipped with a dark-field condenser and an LU plus ELWD 50×/0.55 Nikon Lens in the forward configuration and an LU Plan Fluor 100×A/0.90 Nikon lens in the reflection configuration. A 100 W quartz halogen lamp was used as a light source. A CCD Camera (ThorLabs) was used to collect images directly from the dark field microscope. The scattering spectra from single vertical rods as well as from hexagonally packed vertical arrays were captured by an Acton Micro-Spec 2150i imaging spectrometer fitted with a PIXIS 1024F CCD. The collected signal was finally analysed with Igor software to subtracted background scattering.

To collect images of the reflected and refracted light from large area vertical arrays, a home built setup was used, as shown in Figure S7. A slide holder (10 mm (L) × 10 mm (W) × 2 mm (H) with 1 mm depth and 1mm width trench in the middle) was 3D printed and attached to an optical fibre holder. The optical fibre holder was further connected to a rotational stage for angle dependent measurements. Two optical fibres (Ocean Optics, fibre diameter: 600 µm, operation wavelength: 200 – 1100 nm) were used for illumination and signal collection. A white light source (Mikropack, DH-2000-BAL, Deuterium and Halogen) was used to illuminate the sample from the side of the slide. The refracted light was collected with a high-resolution Spectrometer (Ocean Optics, HR2000). All measurements were carried out in the dark to minimize the background scattering. The background signal was then subtracted from the spectra collected at each angle.

The absorption spectra of gold nanorod colloids were collected with a standard UV-Vis spectrometer (Agilent 8453). All gold nanorod colloids were diluted to approximately 30 µg/mL. All

digital photos were taken with a digital camera (Canon EOS 200D) equipped with a EFS 18-55 mm lens.

Electron microscopy and Atomic force microscopy

The morphology of the rods was determined by transmission electron microscopy (TEM). To prepare the TEM grid, one drop (approx. 5-10µL) of gold nanorod aqueous solution was drop cast onto a carbon coated, 300 mesh copper grid (Electron Microscopy Sciences). A Tecnai F20 (FEI) TEM was used to image the nanorod at 200 kV accelerating voltage. Scanning electron microscopy images were collected with an FEI Nova Nanolab SEM at 5 kV and 1.6 nA current.

The height profile of the vertical gold nanorod array was ascertained by atomic force microscopy (AFM). An MFP-3D AFM (Asylum Research) loaded with silicon cantilevers (AC240TS-R3, Asylum Research) was used to image the array in either contact or tapping mode.

ACKNOWLEDGEMENTS

The authors thank the Australian Research Council for support under grants CE170100026, LP160100054, LE110100161, and LF100100117. We thank Anthony Chessman and the Melbourne Centre for Nanofabrication (MCN) in the Victorian Node of the Australian National Fabrication Facility (ANFF) for access to EBL. We thank the Melbourne Advanced Microscopy Facility (Bio 21, The University of Melbourne) for electron microscopy access. This work was performed in part at the Melbourne Centre for Nanofabrication (MCN) in the Victorian Node of the Australian National Fabrication Facility (ANFF).

AUTHOR CONTRIBUTIONS

HZ synthesised gold nanoparticles, designed the experiments and experimental devices, built the experiment set-up, performed the assembly experiments, performed the COMSOL simulation and co-wrote the manuscript. YL developed and performed the DPD simulations and helped write the manuscript. FS performed the COMSOL simulation. JC and FM carried out nanofabrication of the ITO-PMMA template by EBL. EA conceived the experimental procedures, helped with the COMSOL simulation and explanation and helped write the manuscript. CK synthesised gold nanoparticles, designed the surface chemistry and assisted with assembly experiments, and helped write the manuscript. AWC supervised the DPD simulations and helped write the manuscript. AR oversaw the optical measurements and helped write the manuscript. PM conceived the research, supervised the research work and co-wrote the manuscript.

ASSOCIATED CONTENT

The Supporting Information is available, DOI:

This includes additional information on gold nanorod morphology and spectroscopy characterization, additional SEM characterization of vertical gold nanorod arrays, additional information on the dipole induced in the gold and associated COMSOL simulation, and additional information about the DPD model and simulations.

COMPETING FINANCIAL INTERESTS

The authors declare no competing financial interests.

REFERENCES

[1] a) I. Pastoriza-Santos, C. Kinnear, J. Pérez-Juste, P. Mulvaney, L. M. Liz-Marzán, *Nat. Rev. Mater.* **2018**, 3, 375; b) Y. Huang, W. Li, M. Qin, H. Zhou, X. Zhang, F. Li, Y. Song, *Small* **2017**, 13; c) S. Shi, T. P. Russell, *Adv. Mater.* **2018**, 30; d) Y. Dong, E. M. Akinoglu, H. Zhang, F. Maasoumi, J. Zhou, P. Mulvaney, *Adv. Funct. Mater.* **2019**, 0, 1904290.

[2] A. Biswas, I. S. Bayer, A. S. Biris, T. Wang, E. Dervishi, F. Faupel, *Adv. Colloid Interface Sci.* **2012**, 170, 2.

[3] a) W. Lu, C. M. Lieber, *Nat. Mater.* **2007**, 6, 841; b) H. Zhang, C. Kinnear, P. Mulvaney, *Adv. Mater.* **2019**, 0, 1904551.

[4] a) M. A. Boles, M. Engel, D. V. Talapin, *Chem. Rev.* **2016**, 116, 11220; b) E. V. Shevchenko, D. V. Talapin, N. A. Kotov, S. O'Brien, C. B. Murray, *Nature* **2006**, 439, 55; c) J. Henzie, M. Grünwald, A. Widmer-Cooper, P. L. Geissler, P. Yang, *Nat. Mater.* **2012**, 11, 131; d) T. P. Bigioni, X.-M. Lin, T. T. Nguyen, E. I. Corwin, T. A. Witten, H. M. Jaeger, *Nat. Mater.* **2006**, 5, 265.

[5] a) V. Flauraud, M. Mastrangeli, G. D. Bernasconi, J. Butet, D. T. Alexander, E. Shahrabi, O. J. Martin, J. Brugger, *Nat. Nanotechnol.* **2017**, 12, 73; b) C. Kuemin, R. Stutz, N. D. Spencer, H. Wolf, *Langmuir* **2011**, 27, 6305; c) C. Kuemin, L. Nowack, L. Bozano, N. D. Spencer, H. Wolf, *Adv. Funct. Mater.* **2012**, 22, 702; d) S. Siavoshi, C. Yilmaz, S. Somu, T. Musacchio, J. R. Upponi, V. P. Torchilin, A. Busnaina, *Langmuir* **2011**, 27, 7301; e) M. Asbahi, S. Mehraeen, F. Wang, N. Yakovlev, K. S. L. Chong, J. Cao, M. C. Tan, J. K. W. Yang, *Nano Lett.* **2015**, 15, 6066.

[6] a) C. Kinnear, J. Cadusch, H. Zhang, J. Lu, T. D. James, A. Roberts, P. Mulvaney, *Langmuir* **2018**, 34, 7355; b) D. Nepal, M. S. Onses, K. Park, M. Jespersen, C. J. Thode, P. F. Nealey, R. A. Vaia, *ACS Nano* **2012**, 6, 5693; c) S. G. Jang, E. J. Kramer, C. J. Hawker, *J. Am. Chem. Soc.* **2011**, 133, 16986.

[7] a) R. Pethig, *Biomicrofluidics* **2010**, 4, 022811; b) Q. Wang, A. A. D. Jones, J. A. Gralnick, L. Lin, C. R. Buie, *Sci. Adv.* **2019**, 5, eaat5664; c) B. H. Lapizco-Encinas, *ELECTROPHORESIS* **2019**, 40, 358.

[8] a) M. A. Huergo, C. M. Maier, M. F. Castez, C. Vericat, S. Nedev, R. C. Salvarezza, A. S. Urban, J. Feldmann, *ACS Nano* **2016**, 10, 3614; b) A. S. Urban, S. Carretero-Palacios, A. A. Lutich, T. Lohmüller, J. Feldmann, F. Jäckel, *Nanoscale* **2014**, 6, 4458; c) J. Do, M. Fedoruk, F. Jäckel, J. Feldmann, *Nano Lett.* **2013**, 13, 4164; d) A. S. Urban, A. A. Lutich, F. D. Stefani, J. Feldmann, *Nano Lett.* **2010**, 10, 4794.

[9] a) J. Lim, C. Lanni, E. R. Evarts, F. Lanni, R. D. Tilton, S. A. Majetich, *ACS Nano* **2011**, 5, 217; b) J. Ge, Y. Hu, M. Biasini, W. P. Beyermann, Y. Yin, *Angew. Chem., Int. Ed.* **2007**, 46, 4342; c) M. Wang, L. He, W. Xu, X. Wang, Y. Yin, *Angew. Chem., Int. Ed.* **2015**, 54, 7077.

[10] a) P. Sarkar, P. S. Nicholson, *J. Am. Ceram. Soc.* **1996**, 79, 1987; b) J. H. Dickerson, A. R. Boccaccini, *Electrophoretic deposition of nanomaterials*, Springer, **2011**; c) K. W. Song, R. Costi, V. Bulović, *Adv. Mater.* **2013**, 25, 1420.

[11] a) A. A. Shah, H. Kang, K. L. Kohlstedt, K. H. Ahn, S. C. Glotzer, C. W. Monroe, M. J. Solomon, *Small* **2012**, 8, 1551; b) A. A. Shah, M. Ganesan, J. Jocz, M. J. Solomon, *ACS Nano* **2014**, 8, 8095.

[12] a) M. Giersig, P. Mulvaney, *Langmuir* **1993**, 9, 3408; b) D. C. Prieve, P. J. Sides, C. L. Wirth, *Curr. Opin. Colloid Interface Sci.* **2010**, 15, 160; c) X. Xiong, P. Makaram, A. Busnaina, K. Bakhtari, S. Somu, N. McGruer, J. Park, *Appl. Phys. Lett.* **2006**, 89, 193108; d) F. Qian, A. J. Pascall, M. Bora, T. Y.-J. Han, S. Guo, S. S. Ly, M. A. Worsley, J. D. Kuntz, T. Y. Olson, *Langmuir* **2015**, 31, 3563.

[13] K. J. M. Bishop, A. M. Drews, C. A. Cartier, S. Pandey, Y. Dou, *Langmuir* **2018**, DOI: 10.1021/acs.langmuir.7b02946.

[14] H. Zhang, J. Cadusch, C. Kinnear, T. James, A. Roberts, P. Mulvaney, *ACS Nano* **2018**, 12, 7529.

[15] a) R. W. O'Brien, L. R. White, *J. Chem. Soc., Faraday Trans. 2* **1978**, 74, 1607; b) O. O. Van der Biest, L. J. Vandeperre, *Annu. Rev. Mater. Sci.* **1999**, 29, 327; c) R. J. Hunter, *Zeta potential in colloid science: principles and applications*, Academic press, **2013**.

[16] a) B. M. I. van der Zande, G. J. M. Koper, H. N. W. Lekkerkerker, *J. Phys. Chem. B* **1999**, 103, 5754; b) A. Singh, N. J. English, K. M. Ryan, *J. Phys. Chem. B* **2013**, 117, 1608; c) A. M. Zhivkov, B. M. I. van der Zande, S. P. Stoylov, *Colloids Surf., A* **2002**, 209, 299; d) N. J. Greybush, K. Charipar, J. A. Geldmeier, S. J. Bauman, P. Johns, J. Naciri, N. Charipar, K. Park, R. A. Vaia, J. Fontana, *ACS Nano* **2019**, 13, 3875; e) A. Singh, N. J. English, K. M. Ryan, *J. Phys. Chem. B* **2012**, 117, 1608.

[17] A. I. Väkeväinen, R. J. Moerland, H. T. Rekola, A. P. Eskelinen, J. P. Martikainen, D. H. Kim, P. Törmä, *Nano Lett.* **2014**, 14, 1721.

[18] J. L. Anderson, *Annual review of fluid mechanics* **1989**, 21, 61.

[19] a) W. Ahmed, E. S. Kooij, A. van Silfhout, B. Poelsema, *Nano Lett.* **2009**, 9, 3786; b) P. Zijlstra, M. van Stee, N. Verhart, Z. Gu, M. Orrit, *Phys. Chem. Chem. Phys.* **2012**, 14, 4584.

[20] Y. Liu, A. Widmer-Cooper, *J. Chem. Phys.* **2019**, 150, 244508.

[21] a) S. K. Meena, M. Sulpizi, *Langmuir* **2013**, 29, 14954; b) S. K. Meena, M. Sulpizi, *Angew. Chem., Int. Ed.* **2016**, 55, 11960.

[22] J. M. Luther, H. Zheng, B. Sadtler, A. P. Alivisatos, *J. Am. Chem. Soc.* **2009**, 131, 16851.

[23] S. Xu, D. Liu, Q. Zhang, Q. Fu, *Composites Science and Technology* **2018**, 156, 117.

[24] X. Ye, C. Zheng, J. Chen, Y. Gao, C. B. Murray, *Nano Lett.* **2013**, 13, 765.

TOC Text

Electrophoretic deposition (EPD) of nanocrystals can be used to fabricate arrays of single, vertically oriented, gold nanorods. The orientation is controlled by the applied electric field, rod aspect ratio and electrolyte composition. The resultant arrays can be used to create tunable optical filters.